ELSEVIER

Contents lists available at ScienceDirect

Journal of Controlled Release

journal homepage: www.elsevier.com/locate/jconrel





Evaluation of chemical disposition in skin by stimulated Raman scattering microscopy

Panagiota Zarmpi ^{a,1}, Dimitrios Tsikritsis ^{b,1}, Jean-Luc Vorng ^b, Natalie A. Belsey ^{b,c}, Annette L. Bunge ^d, Timothy J. Woodman ^a, M. Begoña Delgado-Charro ^a, Richard H. Guy ^{a,*}

- ^a University of Bath, Department of Life Sciences, Claverton Down, Bath BA2 7AY, UK
- ^b National Physical Laboratory, Teddington TW11 0LW, UK
- ^c University of Surrey, School of Chemistry & Chemical Engineering, Guildford GU2 7XH, UK
- ^d Colorado School of Mines, Department of Chemical & Biological Engineering, Golden, CO 80401, USA

ARTICLE INFO

Drug disposition in skin

Keywords: Raman spectroscopy Stimulated Raman scattering microscopy In vitro permeation test Cutaneous pharmacokinetics

ABSTRACT

Tracking drug disposition in the skin in a non-destructive and at least semi-quantitative fashion is a relevant objective for the assessment of local (cutaneous) bioavailability. Confocal Raman spectroscopy has been shown potentially useful in this regard and, importantly, recent advances have enabled the presence of applied chemicals in the viable epidermis below the stratum corneum (SC) to be determined without ambiguity and having addressed the challenges of (a) background signals from endogenous species and noise and (b) signal attenuation due to absorption and scattering. This study aimed to confirm these observations using a different vibrational spectroscopy approach - specifically, stimulated Raman scattering (SRS) microscopy - and the more conventional in vitro skin penetration test (IVPT). SRS is a nonlinear optical imaging technique which enables more precise location of the skin surface and enhanced skin depth resolution relative to confocal Raman microscopy. The method can also probe larger areas of the sample under investigation and identify the localization of the permeating chemical in specific structural components of the skin. Here, SRS was shown capable of tracking the uptake and distribution of 4-cyanophenol (CP), the same model compound used in the recent confocal Raman investigation, at depths beyond the SC following skin treatment with different vehicles and for different times. The SRS results correlated well with those from the confocal Raman experiments, and both were consistent with independent IVPT measurements. Acquired images clearly delineated CP preference for the intercellular lipid layers of the SC relative to the corneocytes. The stage is now set to apply these and other correlative techniques to examine commercial drug products.

1. Introduction

Raman spectroscopy is under examination as a tool with which to assess topical drug bioavailability (BA) and dermatological product bioequivalence (BE) [1–4]. Particular challenges relate to the requirement for at least semi-quantification of drug levels within the viable epidermis below the stratum corneum (SC) and how to correct for Raman signal attenuation as a function of skin depth. Having recently described a strategy to address the latter [3], it is equally important to ensure the extent to which the results from experiments using confocal Raman spectroscopy - which showed that a topically applied chemical was detectable within the living layers of the skin and close(r) to the site of pharmacological action - can be confirmed and validated by

measurements acquired with stimulated Raman scattering microscopy (SRS) [1,5] and the more widely accepted in vitro skin permeation test (IVPT) methodology. Specifically for SRS, the principal aim is to demonstrate that the technique can replicate the permeation profiles into the skin, as functions of time and depth, of the same 'model' compound used in the confocal Raman investigation when applied from formulations with distinctly different performances in terms of delivery. The chemical chosen was 4-cyanophenol (CP), which has a strong Raman signal (C=N vibration) at 2230 cm⁻¹ where the skin is spectroscopically-silent.

SRS is an optical technique that allows non-invasive, non-destructive, and label-free chemical imaging and enables fast spatiotemporal and potentially quantitative identification of drug distribution in biological

E-mail address: r.h.guy@bath.ac.uk (R.H. Guy).

 $^{^{\}star}$ Corresponding author.

¹ These authors contributed equally to this research.

samples, including the skin and nail [1,5-8]. As well as tracking the distribution of endogenous and exogenous species in the tissue, SRS can also shed light on the 'metamorphosis' of a drug product on the skin surface post-application (and, in particular, changes in the physical form of the active pharmaceutical ingredient (API)) and reveal the mechanisms by which APIs and, in some cases, excipients can permeate across the skin. Additionally, SRS can be combined and correlated with multiphoton imaging modalities such as 2-photon excitation fluorescence (TPEF) and second harmonic generation (SHG) that can provide insights into the structural microenvironment of the tissue. In contrast to confocal Raman, the SRS technique coherently tunes two laser beam frequencies (the socalled Stokes and pump beams) and targets a specific molecular vibration of interest. The resulting enhancement of the SRS signal enables significantly faster imaging compared to spontaneous Raman [5]. In this way, consecutive on-resonance signals can be obtained at a single frequency in multiple scans (but may require spurious signals, due to 2photon absorption, photothermal lensing and cross-phase modulation to be identified and removed at nearby off-resonance frequencies [5]). Furthermore, lambda (λ) scans can be acquired over a range of wavenumbers permitting spectra that contain information of multiple components to be retrieved in a single scan.

SRS has already made significant contributions in skin and nail research, notably in the characterisation and chemical composition of these barriers [9,10] and in demonstrating how the uptake of different compounds, in terms of amount and rate, can be at least semi-quantified using the technique [1,6-8]. In parallel, label-free imaging with SRS combined with a sophisticated unmixing approach to circumvent background interference (from skin and formulation excipients) has enabled the Raman signal from the compound of interest (which was CP again) to be clearly defined [11]. In the research reported here, recently published confocal Raman data describing the permeation of CP into the skin from different laboratory-made formulations are validated using SRS imaging and conventional in vitro skin permeation test (IVPT) experiments. It is confirmed that the procedures developed can generate results which may ultimately be useful for the derivation of metrics related to the local bioavailability of APIs within the living tissue layers of the skin and, in particular, the viable epidermis, where many dermatological drugs have their site of action).

2. Materials and methods

2.1. Materials

4-Cyanophenol (CP), propylene glycol (PG) and all other solvents and chromatography reagents were purchased from Sigma Aldrich (Dorset, UK). Fresh abdominal porcine skin from two animals was obtained from a tissue supplier and then dermatomed (Zimmer®, Hudson, OH, USA) within 48 h of slaughter to a nominal thickness of 750 μm . Visually obvious hairs were carefully cut with scissors and the tissue was stored at $-20\,^{\circ}\text{C}$ and thawed shortly before use.

2.2. Ex vivo measurement of CP uptake into skin

The in vitro skin permeation (IVPT) experiments involved application of 300 μL of (a) fully saturated solutions of CP in either 50:50 %v/v water:PG or 90:10 %v/v water:PG (170 and 17 mg/ mL, respectively) for either 1 or 2 h, and (b) fully or 25% saturated solutions of CP in 50:50 % v/v water:PG (170 and 42.5 mg/ mL, respectively) for 6 h. Each formulation was applied to skin mounted in a Franz cell (diffusion area of 2.01 cm²), that was thermostatted at 32 °C; the receptor chamber of the cell (volume = 7.4 mL) was filled with pH 7.4 phosphate-buffered saline (PBS). To limit any significant evaporation of the vehicles, the donor chamber was occluded with Parafilm [Memis Company, Inc., Neenah, USA). At the end of each experiment, residual formulation was cleaned from the skin surface by wiping with standard absorbent paper and the tissue was immediately frozen at $-80\,^{\circ}\text{C}$ for short-term storage

and transport for SRS imaging.

In the same way, conventional IVPT experiments were separately undertaken to measure the distribution of CP in the SC, the remaining epidermis/dermis, and the receptor solution. At the end of each of these experiments, a 1 mL sample of the receptor solution was withdrawn and analysed by high-performance liquid chromatography with UV detection [2] to determine the amount of CP that had permeated the skin during the application period. Residual formulation was again cleaned from the skin surface by wiping with absorbent paper. The disposition of CP in the SC was assessed by sequential adhesive tape-stripping using a previously reported procedure [2]. Typically, 20 tape-strips were taken from which CP was then extracted overnight using a 40:60%v/v methanol:0.1% formic acid aqueous solution (tapes were extracted individually in 3 mL of extraction solvent). CP in the remaining skin (epidermis/dermis) was extracted in the same way using 5 mL of the extraction solvent. Quantification of CP in the SC and the remaining skin used the same HPLC-UV assay [2].

A control skin sample was also prepared in a 6-h IVPT 'experiment' in which no formulation was applied. This control sample served as a blank to confirm the absence of interference in the frequency region of the C \equiv N vibration and to assess SRS signal attenuation as a function of depth into the skin. A small portion of this untreated sample was taken, fixed at $-25\,^{\circ}$ C and cryo-microtomed (Leica CM1850 cryostat, Germany) for SRS analysis in "cross-section" [3].

2.3. Stimulated Raman Scattering Microscopy (SRS)

For "top-down" image acquisition [3], the skin samples were removed from the dry ice, in which they had been transported, and then rapidly frozen by dipping into liquid nitrogen for a few seconds. Subsequently, the tissue block was cut horizontally with a scalpel to create a thin slice (\sim 100–200 µm) containing the SC and part of the viable skin. An imaging spacer of double-sided adhesive tape (Grace Bio-Labs, SecureSealTM, Sigma Aldrich, USA) was placed in the middle of a glass slide and the resulting skin sample was positioned in the circular opening with the SC in direct contact with the glass side. The sample was then overlaid with a coverslip to minimise tissue dehydration during the experiment [6]. The sample was secured on the stage with a clamp to prevent movement and flexing of the coverslip. During sample preparation and SRS imaging, the samples were kept at room temperature. SRS, SHG and TPEF microscopy images were acquired on a Leica SP8 laser scanning microscope (Leica Microsystems, Wetzlar, Germany) coupled to a PicoEmerald-S laser system (APE, Berlin, Germany). The PicoEmerald-S generates two pulsed 2 ps laser beams: a 1031.2 nm Stokes beam which was spatially and temporally overlapped with a tuneable pump beam. The Stokes beam was modulated at 20 MHz and stimulated Raman loss signals were detected using a silicon-based detector and lock-in amplifier (UHFLI, Zurich instruments, Zurich, Switzerland). A second channel was utilised to measure second harmonic and emitted fluorescence signals using photomultiplier tubes.

Images were acquired with a water immersion $25\times/0.95$ numerical aperture (NA) objective lens. Coherent anti-Stokes Raman scattering (CARS), TPEF and SHG were detected in the epi direction; in contrast, SRS imaging was performed in the forward direction, and signals were collected through a condenser lens (Leica S1 50,515) with a NA of 0.90. The system was checked daily for alignment (temporal and spatial overlap) of the contributing beams, with the use of in-house standards.

The laser power used was 30% (36 mW and 11.7 mW at the sample for the Stokes and pump beams, respectively), which was selected to produce a satisfactory signal-to-noise ratio while minimising sample dehydration and shrinking. The pump beam was tuned to achieve SRS contrast at 2235, 1666 and 2850 cm⁻¹ to obtain the on-resonance signals of CP (C \equiv N stretching), Amide *I* (C \equiv O stretching) and skin lipids (CH₂ stretching), respectively. Spurious signals were identified and removed by acquiring and subtracting the corresponding off-resonance frequencies of 2292, 1723 and 2600 cm⁻¹, respectively.

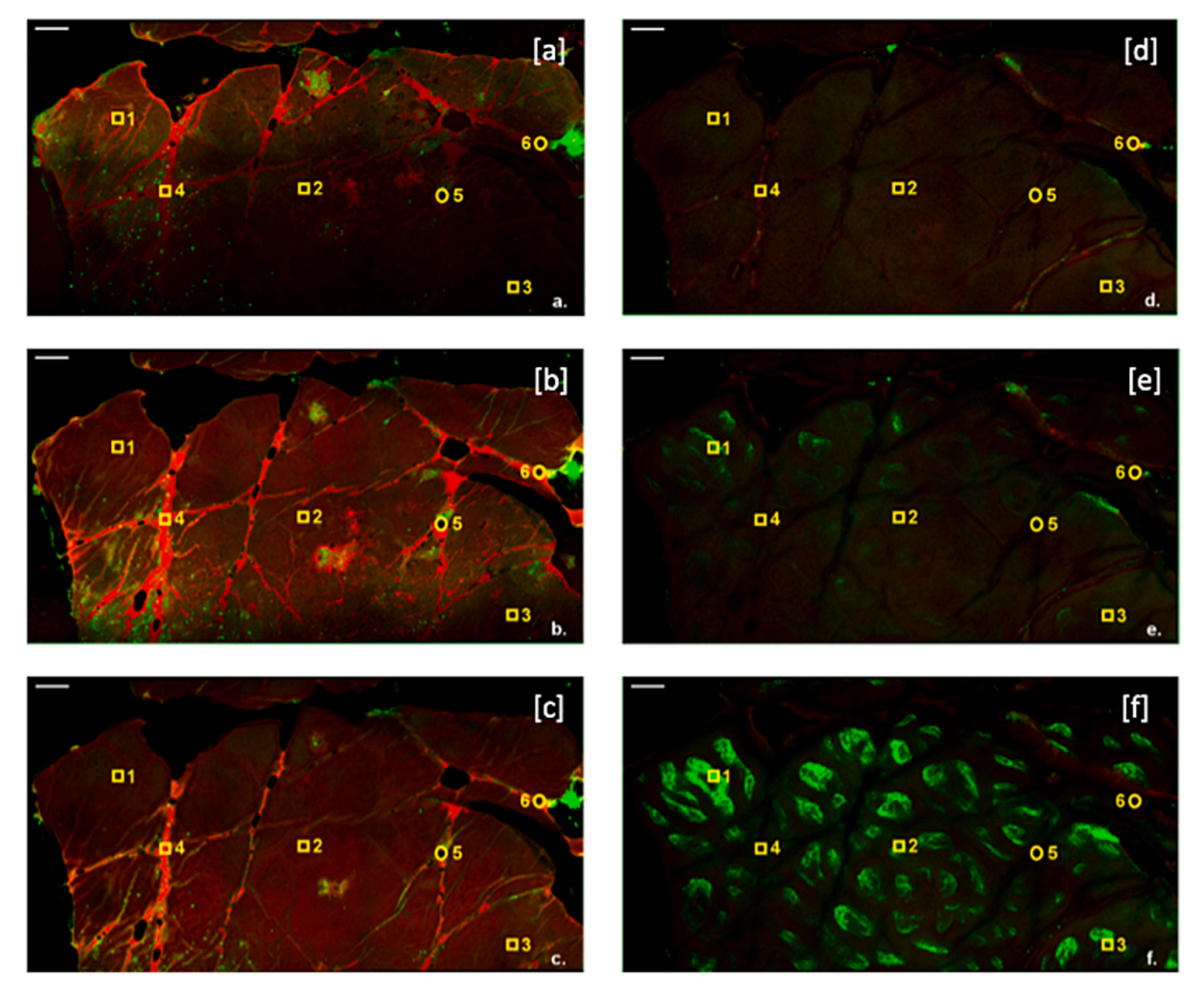


Fig. 1. Multi-tile scans of untreated porcine skin showing the CH_2 SRS signal distribution (in red) and the SHG signals, in a separate channel (in green), as function of depth: images [a], [b], [c], [d], [e], and [f] represent 0, 5, 10, 25, 35 and 45 μ m depth, respectively. The average pixel intensity of selected regions of interest (30 \times 30 pixels, numbered 1–6; indicated as squares except for apparent appendageal openings designated by circles) are calculated as gray scale values as a function of depth. The scale bar corresponds to 100 μ m. (For interpretation of the references to colour in this figure legend, the reader is referred to the web version of this article.)

Complementary SHG imaging was performed at 398.8 nm (collection wavelength) correlatively with the $2851~{\rm cm}^{-1}$ (797.8 nm excitation wavelength). Acquiring the best quality SRS images required individual optimisation of the SRS silicon detector gain settings: 72.2~V, 546.2~V and 53.6~V for CP, Amide I and lipids, respectively. For SHG collection, a gain of 1250~V was applied to the photomultiplier tube.

These values were consistently applied to permit comparison between dosed and control samples. The values were optimised using a skin sample exposed to the highest amount of CP (i.e., following the 6-h application of the fully saturated CP in 50:50 %v/v water:PG). Consequently, the resulting images were free from signal saturation. Multi-tile scans were generated by use of the "mosaic merge" function that acquires and stitches together single tiles (465 \times 465 μm). 3D image stacks were acquired using a depth increment of 0.5 μm , unless stated otherwise.

For image acquisition of the skin in "cross-section", the sample was positioned on a glass side similar to the "top-down" approach [3]. Instrument parameters were as above except that the gains used were 60 V, 60 V and 20 V for SRS of CP, Amide I, and skin lipids, respectively, and 1000 V for SHG.

2.4. Data analysis

All SRS images were processed using ImageJ [12]. The "top-down" images for each signal were stacked as a function of depth. Because all channels were acquired sequentially, small translational drifts in the sample position were observed. However, image registration was not performed because, given the inhomogeneity in tissue thickness, different drifts were observed across each image (x and y direction) and depth stack (z direction) [5]. Z-stacks acquired at the off-resonance, control wavenumber were subtracted from the on-resonance SRS images for CP, Amide I, and skin lipids, using the image calculator tool. To enable comparison of the images acquired from skin samples that had been treated with different formulations and/or for different times, image display settings were consistently applied for the CP, Amide I and CH2 signals. These processed image stacks were then colour-merged. A similar approach was followed to process the "cross-section" images. The optically sliced "top-down" images were obtained using the ImageJ volume viewer tool.

For data analysis, on- and off-resonance depth scans were colour-

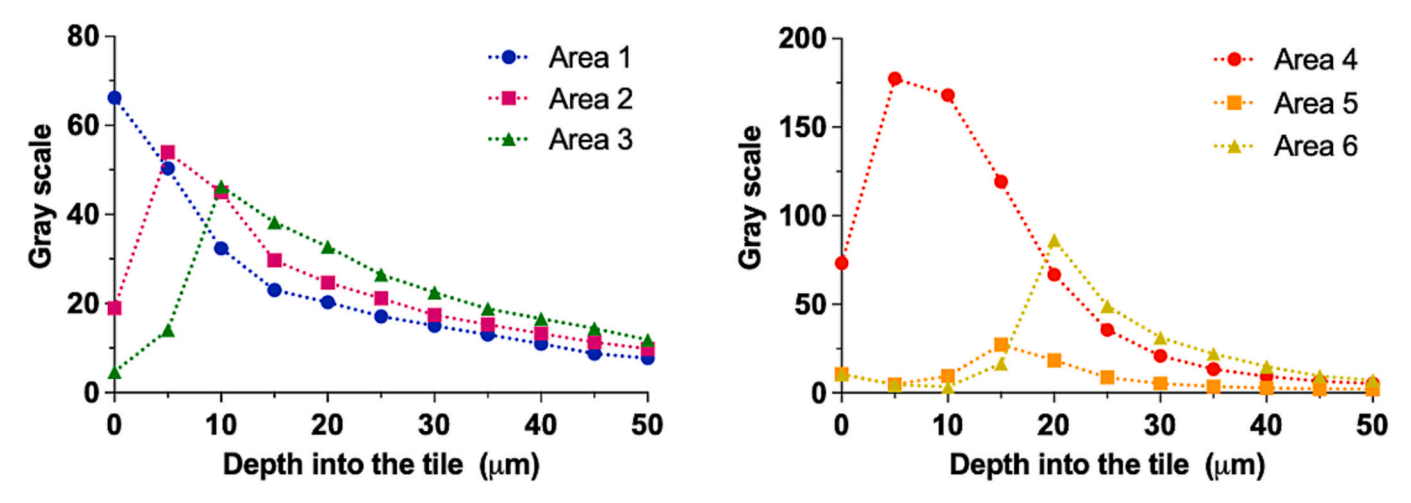


Fig. 2. Variation in the CH_2 gray scales as function of apparent depth into the skin at the 6 areas highlighted in Fig. 1. The variability likely reflects small differences in the levels of skin lipids and proteins (reflected by $-CH_2$ signal intensities) and fall within the typical range previously reported [3].

stacked in one tile. SRS signal intensity was assessed from the gray scale values of each component in 6 selected representative areas as a function of depth through the map (i.e., in the z direction): (a) multi-tile scans $(30 \times 30 \text{ pixels})$ visualised the whole tissue that was placed on the microscope slide, including crevices and appendages; and (b) single-tile scans (20×20 pixels) visualised one smaller area from the multi-tile scan, excluding crevices and appendages. The resulting, acquired gray scale signals of CP, Amide I and skin lipids, corrected by the corresponding off-resonance values, were graphically displayed as function of depth and any drifts observed in the 6 areas examined were adjusted accordingly, by monitoring the maximum rate of change of each component. A similar approach was followed to process the "cross-section" images, by interrogating six 1 pixel-width lines. Normalised CP gray scale values were calculated by dividing the off-resonance corrected signal by the corresponding Amide I value. Gray scale or normalised gray scale values were then plotted as function of depth (in μ m) into the skin using GraphPad Prism 5 (version 9.3.1, San Diego, CA).

To calculate the exponential loss of measured signal from attenuation with depth, the natural log-transformed gray scales of the Amide I signal from the untreated tissue were linearly regressed as a function of skin depth and assessed in terms of goodness of fit (r^2) using GraphPad Prism 5 (version 9.3.1, San Diego, CA). The same approach was used to assess the signal attenuation of the off resonances for Amide I, CH₂ and CP.

3. Results

3.1. SRS-assessed skin heterogeneity and surface location

A representative, multi-tile depth scan of untreated skin is shown in Fig. 1. In this case, only the SRS CH₂ signal, predominantly from skin lipids, and the SHG channel were imaged to ensure that the scan time required did not induce significant tissue dehydration. Images [a] through [f] are depth increments of the same skin area. Image [a] shows that the tissue has a non-constant thickness as only half of the skin surface is visible in the upper (and obviously thicker) part of the image. As the focus moves 5 and then 10 µm deeper into the tissue (images [b] and [c], respectively), the SRS signal for CH₂ contrast is detected across the entirety of the skin. This inhomogeneity is both inherent in the biological samples studied and almost certainly introduced during the sectioning involved in sample preparation. It is important, therefore, to correctly locate the skin surface when conducting depth scans to ensure that the subsequent data analysis is objectively performed. Thus, image [a] in Fig. 1 represents the first stack visualised in the experiment; subsequently, images [b], [c], [d], [e], and [f] correspond to the stacks recorded, respectively, at 5, 10, 25, 35 and 45 μm below image [a].

Raman signals from endogenous skin proteins and lipids are ex-

pected to show a sharp increase [13] as the laser focus moves from the air and onto the skin surface and this is confirmed in Fig. 2, which shows the changes in the CH₂ gray scales in the 6 mapped areas identified by number in Fig. 1. In subsequent, single-tile experiments on either untreated or treated skin, the CH₂ signals were routinely recorded, therefore, and allowed the tissue surface to be identified. The rate of gray scale change in each image z-stack was calculated using:

$$R = \frac{gs_{n+1} - gs_n}{s_{n+1} - s_n} \tag{1}$$

where R is the rate of change of the signal in each image stack, gs is the gray scale of the CH₂ signal, and s_n and s_{n+1} indicate the n^{th} and $(n+1)^{\text{th}}$ image stacks (image stacks in this case are indicative of tissue depth). The skin surface was identified when R achieved a maximum value.

The six sites visualised on the skin include a 'crevice' or invagination (area 4) and what appear to be appendageal openings (areas 5 and 6) (Fig. 1). For the 'crevice', the skin surface manifests a high CH_2 signal suggesting the accumulation of sebum in these regions (Fig. 2). The skin pore openings show maxima in the CH_2 signals at relatively greater depths (Fig. 2). Overall, though, regardless of the structural feature differences at the examined skin areas, the gray scale values (once the surface is located) reached a local maximum and then decreased with increasing depth due to signal attenuation (discussed further below).

The SHG signal showed the opposite behaviour and became stronger in the deeper layers of the skin. Although SHG in biological samples is typically associated with non-centrosymmetric structures linked to the alignment of polar collagen [14], this association in Fig. 1 may be questioned because, in the skin, this structural protein is predominantly present in the dermis (i.e., considerably deeper into the tissue than the $\sim\!50\,\mu\mathrm{m}$ probed in these experiments). However, tissue dehydration may result in a shrinkage of the epidermis, and this would mean that these signals appear earlier than expected. An alternative explanation for the most intense SHG signal being observed in Fig. 1f, in particular, is that it originates from autofluorescence of the sebaceous glands [15]; this is consistent with their anticipated location and with the visual appearance of the structural features revealed, although these structures appear much more densely packed. The combination of the two suggestions is equally plausible.

3.2. Strategy to correct for signal attenuation

The SRS Amide I gray scale "top-down" and "cross-section" measurements from untreated skin samples are in Fig. 3a. The "top-down" data illustrate how the Amide I signal is attenuated with increasing depth due to light absorption and scattering, as demonstrated in a recent report

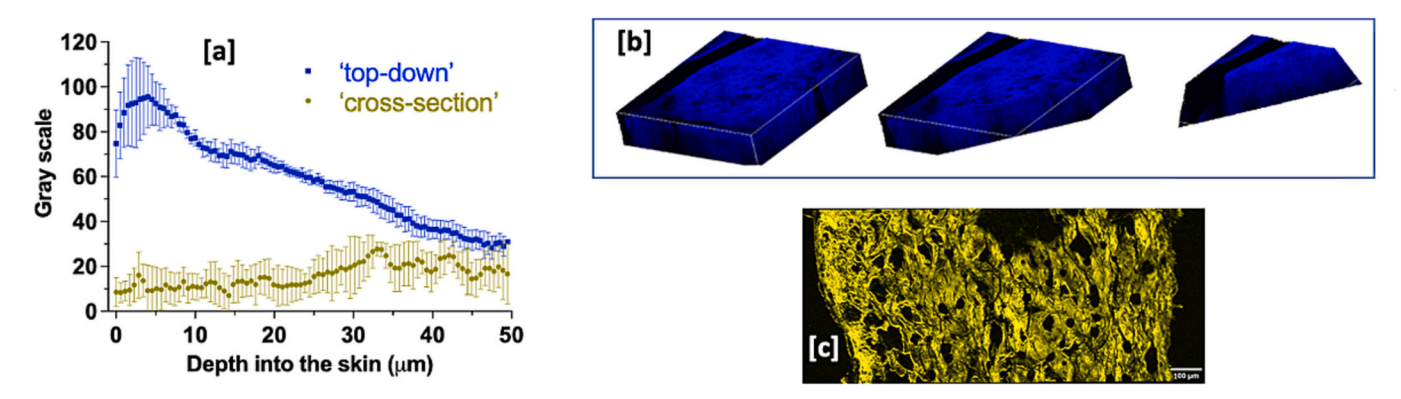


Fig. 3. [a] Amide I signal (average gray scale value, in arbitrary units) measured "top-down" (blue) and in "cross-section" (yellow) by SRS. Data are the means (\pm SD) of measurements from six selected areas (20×20 pixels) in one skin sample. [b] Progressively exposed (blue to black colours indicate high and low Amide I signals, respectively), optically orthogonal slices showing side views of the "top-down" SRS images of the Amide I distribution in untreated skin (field of view is $465 \, \mu \text{m}^2$ and height is $50 \, \mu \text{m}$; see also Supplementary Movie S.1. [c] Typical Amide I signal when skin is examined by SRS in "cross-section"; scale bar = $100 \, \mu \text{m}$. (For interpretation of the references to colour in this figure legend, the reader is referred to the web version of this article.)

using confocal Raman spectroscopy [3]. From the skin surface to a depth of 50 μ m, the average Amide *I* gray scale value reduced by just over 50%. Inspection of the "top-down" stacks presented in Fig. 3b confirm that the Amide *I* signal loss occurred throughout the tissue. Supplementary Movie S.1 shows that, in addition to Amide *I*, attenuation with depth is seen for the CH₂ signals originating primarily from skin lipids.

In contrast, the results from the "cross-section" approach (i.e., measurements of skin depth from the side of the sample to avoid signal attenuation) reveal (in a manner completely consistent with the earlier confocal Raman experiments [3]) that the Amide I signal is relatively constant with depth. The gray scale values were noticeably lower in "cross-section" – especially closer to the surface - because different signal detector gains were used for the two acquisition modes. This is expected because SRS signals are detected in transmission and are therefore impacted by the thickness of the sample. Consequently, the 'top-down' samples require a higher gain voltage to increase signal intensity. A typical SRS "cross-section" image from untreated skin (Fig. 3c) confirms the consistency of the Amide I signal over depths of several hundred microns.

Given that the Amide I determined in 'cross-section' is constant as a function of depth, the signal attenuation constant (β) describing the observed decrease in the signal measured 'top-down' can be calculated assuming a simple exponential decay (Fig. 4). When the 6 'top-down' replicates of the Amide I measurements are modelled in this way, the average β value obtained (with its 95% confidence intervals) is 0.0243 a. u./µm (0.0234–0.0252 a.u./µm) with an $r^2=0.97$. This value is slightly higher than that reported for confocal Raman microscopy (0.0157 a.u./µm with 95% confidence intervals of 0.0101–0.0213 a.u./µm) [3].

It can be observed in Figs. 3 and 4 that the amide I signal exhibits

greater measurement uncertainty near the surface of the skin, as evidenced by the larger error bars. The most likely explanation for this higher variability is the combination of the roughness of the skin's surface coupled with the optical volume of the sample probed during a 'top-down' analysis. At the sample height defined as the surface, some regions within the optical plane will be slightly above the true skin surface, and thus contain voxels for which the optical volume is not entirely filled by material, i.e. resulting in a reduced signal intensity. Whereas, deeper in the skin, the optical volume probed is consistently filled with material. This explanation (rather than inherent variability in the tissue) is consistent with the observation that the error bar magnitude remains more constant throughout the skin depths for the skin cross-section, for which the measurements were determined using single-pixel width line measurements.

3.3. Ex vivo measurement of 4-cyanophenol (CP) uptake into skin by SRS

As a negative control, the SRS signal at $2235 \,\mathrm{cm}^{-1}$, which is the frequency of the C \equiv N stretching vibration, was also recorded in the "top-down" experiments performed on untreated skin. The results, normalised by the corresponding Amide I values, are in Supplementary Fig. S.1 and confirm the absence of any background interference at this frequency.

The SRS-assessed gray scales of Amide I, CP and the CP/Amide I normalised ratio, after 1- and 2-h applications of the fully saturated chemical in solutions of 50:50 and 90:10 %v/v water:PG are presented in Fig. 5. It is observed that the disposition of CP is successfully measured at skin depths below the SC. The attenuation of the Amide I signal as a

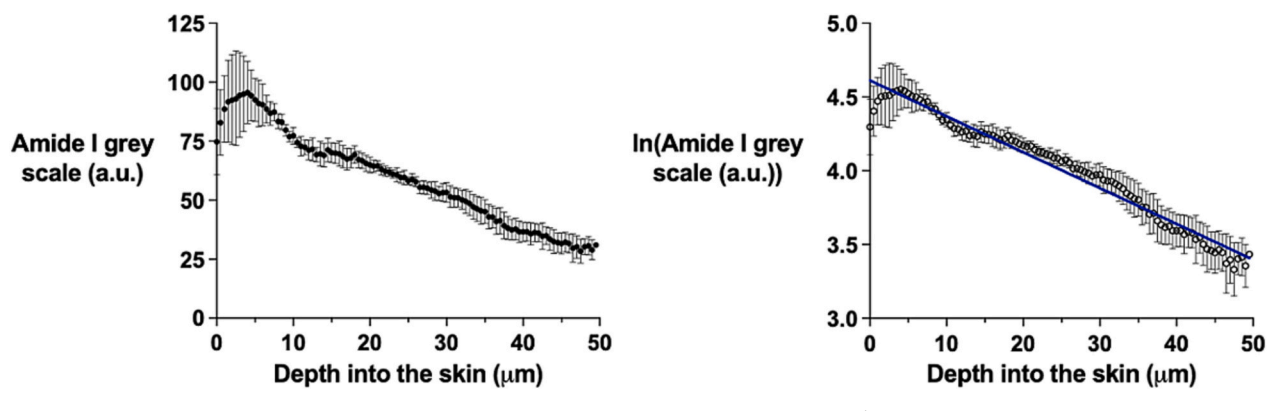


Fig. 4. Maximum Amide I gray scales (geometric means with their 95% confidence intervals) at 1666 cm⁻¹ measured 'top-down' as a function of skin depth (left panel) and the natural logarithmic transformation of the data (means with their 95% confidence intervals; right panel). Data points are calculated from experiments using 6 selected areas in one skin sample.

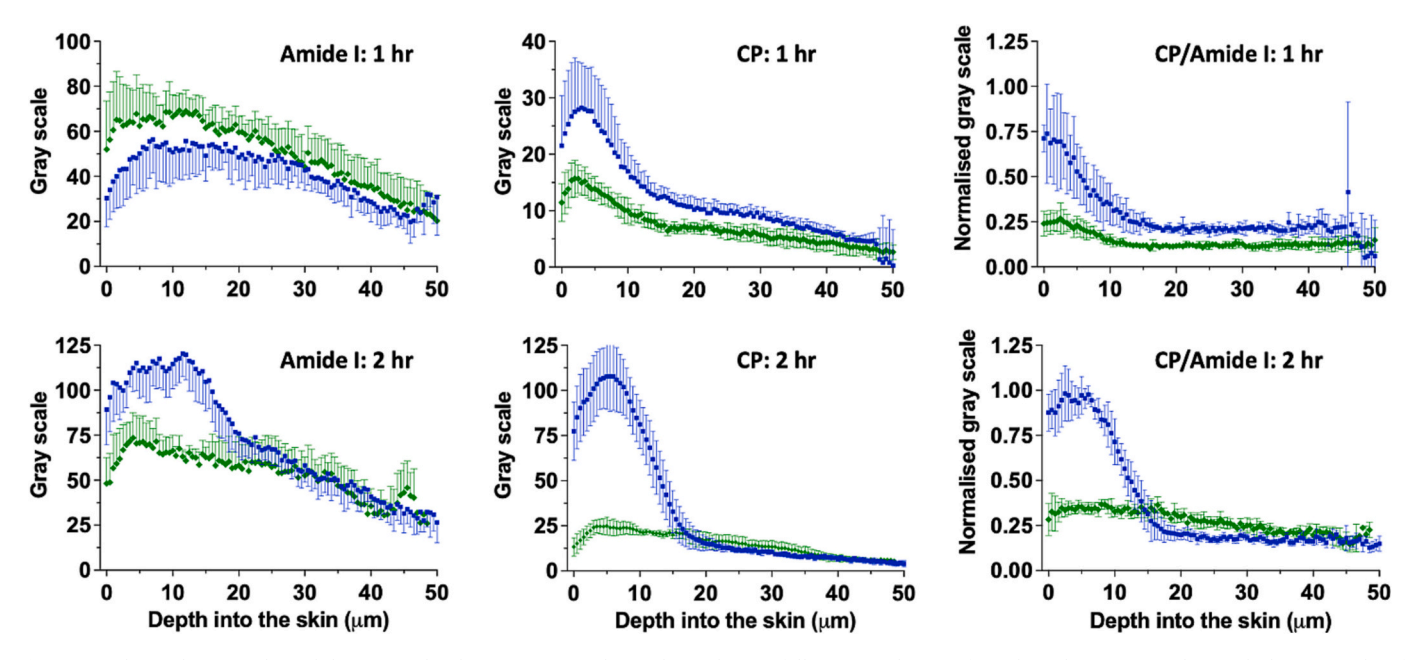


Fig. 5. Amide I and CP signals, and their normalised ratios, measured "top-down" by SRS following application for either 1 h (upper panels) or 2 h (lower panels) of fully saturated solutions of CP in 50:50 (in blue) and 90:10 %v/v water:PG (in green). Data points are the means (\pm SD) of measurements six selected areas in one skin sample per formulation. The 1 h experiments were conducted with skin samples from one pig, while the 2 h measurements were made using tissue from a second pig. (For interpretation of the references to colour in this figure legend, the reader is referred to the web version of this article.)

function of depth is clear (as already demonstrated above); however, the decay of the CP signal is due both to signal attenuation and to the diminishing concentration of the chemical as it is taken up into the skin. Normalisation of the CP signal with the corresponding Amide I values permits signal attenuation to be taken into account and the generation of profiles that are correctly representative of the compound's distribution in the skin at the time of measurement. Figs. 6 and 7, and Supplementary Movies S.2 and S.3, provide examples of the SRS data demonstrating the dynamic evolution of CP uptake into the skin from the two formulations. Because the skin samples were not kept continuously frozen during SRS sample preparation and CP measurements (\sim 2 h), the normalised profiles observed for CP, which has a diffusion lag time of \sim 0.5 h [16], will differ from the profiles at the end diffusion cell experiment.

Fig. 8 presents the corresponding SRS data from the experiment in which fully- and 25%-saturated CP solutions in 50:50 %v/v water:PG were applied for a period of 6 h. As for the results in Fig. 5, these measurements are fully consistent with those reported recently using confocal Raman spectroscopy [3]. The SRS signal of Amide I from the skin following application of both formulations (but particularly apparent for the fully-saturated one) shows a dip in the first few microns before a subsequent increase. Fig. 9 and Supplementary Movie S.4 track these changes which appear to be correlated with the field of view capturing the cornecytes.

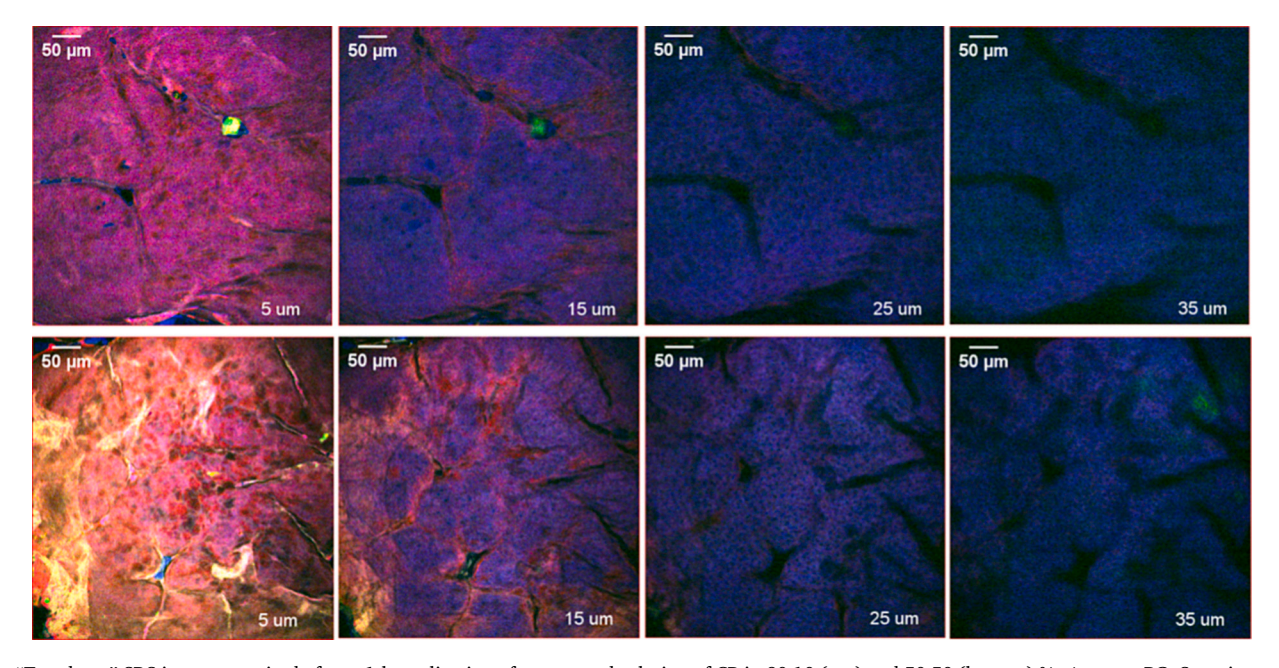


Fig. 6. "Top-down" SRS images acquired after a 1-h application of a saturated solution of CP in 90:10 (top) and 50:50 (bottom) %v/v water:PG. Superimposed SRS signals from CP (yellow), Amide I (blue) and CH_2 (red) in addition to SHG signals (green) are shown as a function of depth (indicated in the bottom right corner of each panel) into the skin; scale $bar = 50 \, \mu m$. (For interpretation of the references to colour in this figure legend, the reader is referred to the web version of this article.)

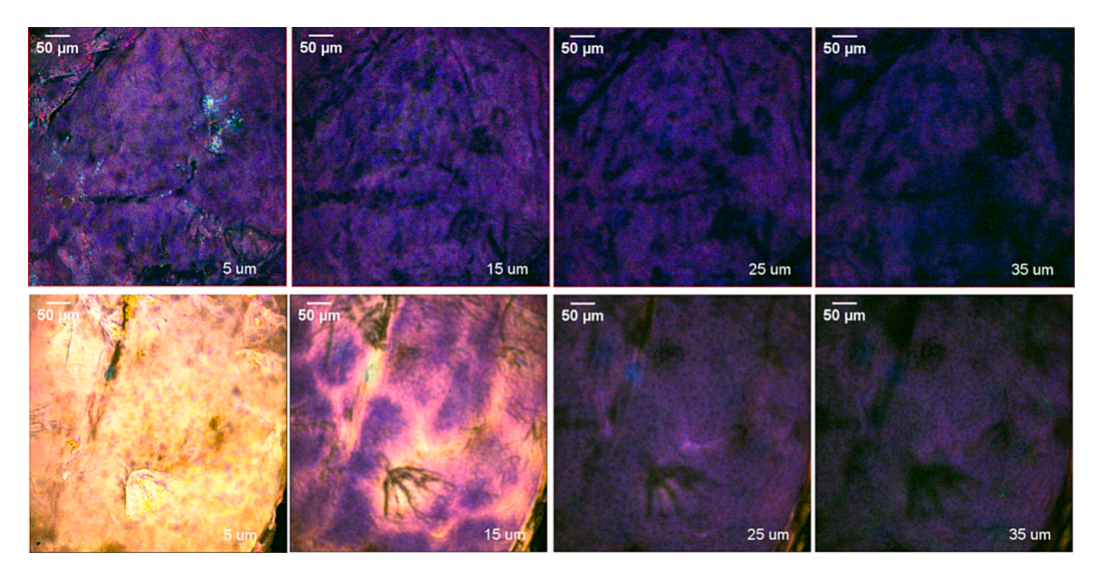


Fig. 7. "Top-down" SRS images acquired after a 2-h application of a saturated solution of CP in 90:10 (top) and 50:50% (bottom) v/v water/PG. Superimposed SRS signals from CP (yellow), Amide I (blue) and CH₂ (red) in addition to SHG signals (green) are shown as a function of depth (indicated in the bottom right of each panel) into the skin; scale bar = 50 μ m. "(For interpretation of the references to colour in this figure legend, the reader is referred to the web version of this article.)

3.4. In vitro skin permeation test (IVPT)

The results from a series of conventional IVPT experiments (that mirrored the SRS studies) are in Fig. 10, which displays the disposition of CP in the SC, the remaining skin (i.e., viable tissue; VT) and the receptor solution (RS) of the diffusion cell after application of the three tested formulations for 1, 2 and 6 h. When the two saturated CP formulations (170 and 17 mg/mL in 50:50 %v/v and 90:10 %v/v water:PG, respectively) were compared, the amounts of penetrant recovered in the SC at 1 and 2 h from the formulation with more PG (235 \pm 75 and 273 \pm 105 $\mu g/cm^2$, respectively) were about double those from the vehicle with less PG (100 \pm 31 and 130 \pm 12 $\mu g/cm^2$, respectively). The quantities found in the VT, on the other hand, were similar for both formulations (approximately 150 and 200 $\mu g/cm^2$ after 1- and 2-h applications, respectively).

The 6-h application experiment compared fully- and 25%-saturated CP formulations in 50:50 water:PG solutions. The former clearly delivered more penetrant into the SC, VT and RS by approximately 3-, 3- and 6-fold, respectively.

4. Discussion

SRS offers a unique opportunity to visualise the skin in considerable detail and to appreciate from the multi-tile scans (Fig. 1) the heterogeneity of its topography and embedded sub-structures (crevices and invaginations, follicles (Supplementary Fig. S.2), sebaceous and sweat glands [17], etc.). It becomes clear, therefore, that the application of a topical formulation is never made to an idealised smooth skin surface

and it is not a surprise, therefore, that drug penetration across the skin is inevitably observed with a certain amount of variability both between and within individuals [18]. Consequently, because this work aimed to attempt a semi-quantitative comparison of chemical uptake into the skin from different formulations applied for different periods of time, imaging was recorded specifically from areas where crevices and appendages were absent. Clearly, however, SRS is a tool with which specific location preferences of the permeating chemical can be probed, the potential for which has already been demonstrated in the literature (e.g., [7,17]) and is primed for further study.

Imaging with SRS also highlights, even over quite short distances, the irregularity (i.e., non-flatness) of even the 'smoother' areas of the skin surface. This general unevenness means that dermatoming the tissue does not guarantee the same thickness across an entire skin sample. The impact of this observation is that the location of the surface must be carefully determined and, as has become the standard approach in the field [8], the steep change in the endogenous species signal from the SC lipids to a maximum value has been used for this purpose. As is evident from Fig. 1 and, in particular, from panels [a], [b] and [c], the CH₂ gray scale values are also particularly good at identifying the accumulation of (presumably) sebaceous lipids in the skin crevices.

Figs. 2 and 3 show that SRS signals originating in the skin - both CH_2 from lipids and Amide I from keratin - collected in the "top-down" experiments become weaker with increasing depth into the skin; that this is due to the expected, progressive absorption and scattering of photons is confirmed by the "cross-section" study which reveals (as exemplified for Amide I (Fig. 3)) that the signal is actually quite constant across the skin when viewed in the same optical plane [5]. Notably, the ability of SRS to

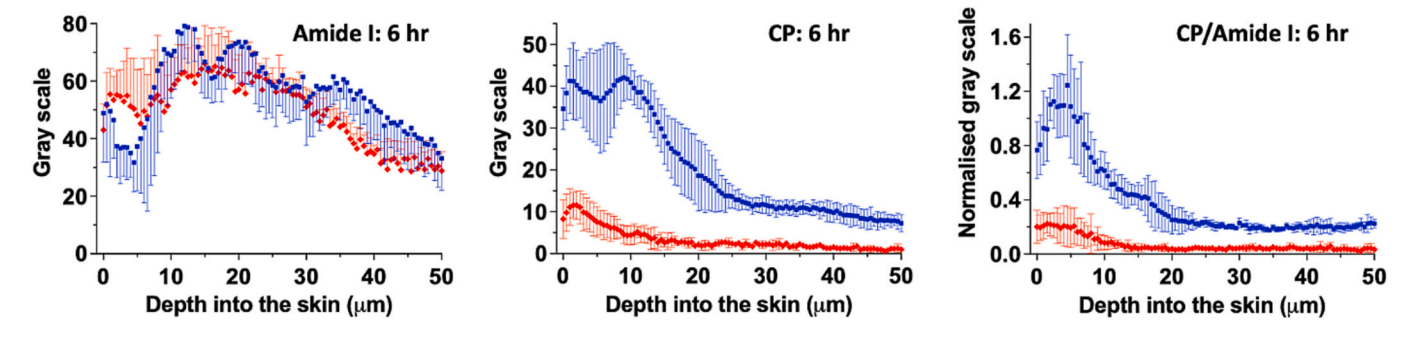


Fig. 8. Amide I and CP signals, and their normalised ratios, measured "top-down" by SRS following application for 6 h of fully- (in blue) and 25%-saturated (in red) solutions of CP in 50:50 %v/v water:PG. Data points are the means (\pm SD) of 6 measurements from one skin sample (from the same pig) per formulation. (For interpretation of the references to colour in this figure legend, the reader is referred to the web version of this article.)

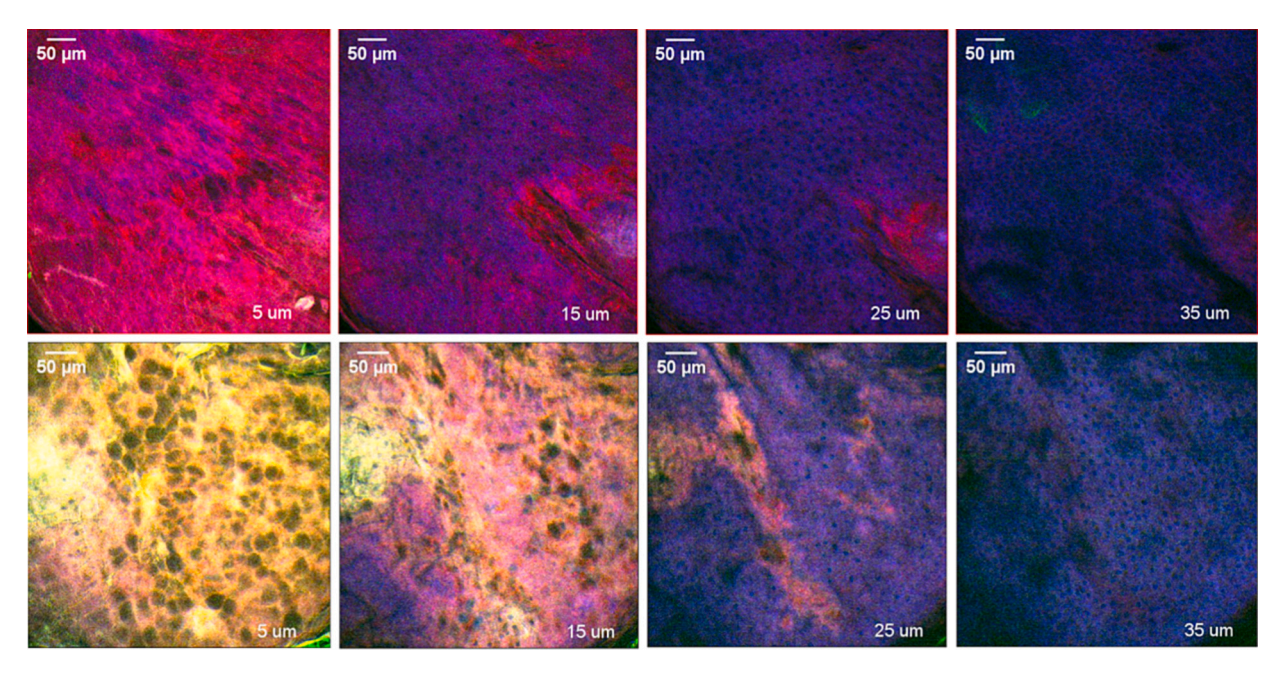


Fig. 9. "Top-down" SRS images acquired after a 6-h application of a saturated solution of CP in 25% (top) and fully (bottom) saturated solution in 50:50 %v/v water: PG. Superimposed SRS signals from CP (yellow), Amide I (blue) and CH_2 (red) in addition to SHG signals (green) are shown as a function of depth into the skin. identified in the bottom right of each panel; scale bar = 50 μ m. "(For interpretation of the references to colour in this figure legend, the reader is referred to the web version of this article.)

rapidly scan relatively large skin areas permits confirmation that the consistency of the Amide I signal is present in a quite uniform manner. It follows that, when tracking CP penetration into the skin in "top-down" mode, the concentration gradient established (high at the surface and then falling away with increasing depth) will be exaggerated by the same signal attenuation seen in the CH_2 and Amide I vibrations. In the same manner as that used in recent confocal Raman work [3], correction for the attenuation of the $C \equiv N$ vibration from CP can be achieved by normalising these signals by the corresponding Amide I values.

It was noted that the exponential decay of the SRS Amide I signal was larger than that observed with confocal Raman [3] (Fig. 4). This may be explained by the fact that the optical volumes interrogated by the two approaches are not the same. SRS is capable of finer optical sectioning (axial resolution of $1 \mu m$), permitting the collection of more data, and with better spatial definition, than confocal Raman. Further, given that SRS detection occurs in forward propagation (i.e., transmission, unlike confocal Raman), signal loss may be greater, particularly when thicker skin pieces are studied. It follows that Amide I can still be used to correct for attenuation with depth, provided that attenuation is similar across different frequencies. To confirm this assumption, the attenuation constants (β , again in units of a.u./ μm) determined from the three offresonance SRS frequencies examined (1723, 2292 and 2600 cm⁻¹ for Amide I, CP and CH₂, respectively) were determined (with their 95% confidence intervals): 0.0210 (0.0223–0.0200; r^2 = 0.92) for Amide I,

0.0204 (0.0213–0.0200; r^2 = 0.95) for CH₂, and 0.0209 (0.0218–0.0200; r^2 = 0.95) for CP. There was no statistical difference between these values nor with that for the Amide I (1-way ANOVA). The similarity of the β values for the on- and off-resonance Amide I attenuation provides additional support that concentration of the species contributing to this signal is constant as function of depth. Furthermore, as the SRS attenuation of the other off-resonance signals at distinctly different frequencies was similar, there is strong support for the CP value of β to be the same as that of Amide I (as was indeed the case for the previous confocal Raman results [3]). It may also be reiterated that the normalisation procedure adopted also permits day-to-day instrumental variability to be taken into account, as well as that originating between skin samples of different thickness.

The areas under the normalised CP versus depth data (AUC_z from 0 to 50 μ m) in Figs. 5 and 8 are collected in Table 1 and provide a metric of skin uptake measured in the SRS experiments with which to compare the different formulations used and the impact of application time. It was also possible to compare these SRS AUC_z results with the corresponding values recently reported using confocal Raman [3].

Although the two fully saturated solutions would normally be expected to deliver the same amount of CP, the data at 1 and 2 h show that this is not the case, and that the 50:50 %v/v water:PG formulation outperforms the 90:10 (Fig. 5). The AUC_z ratios (50:50/90:10) were 2.0 and 1.4 at 1 and 2 h, respectively; the corresponding values from the

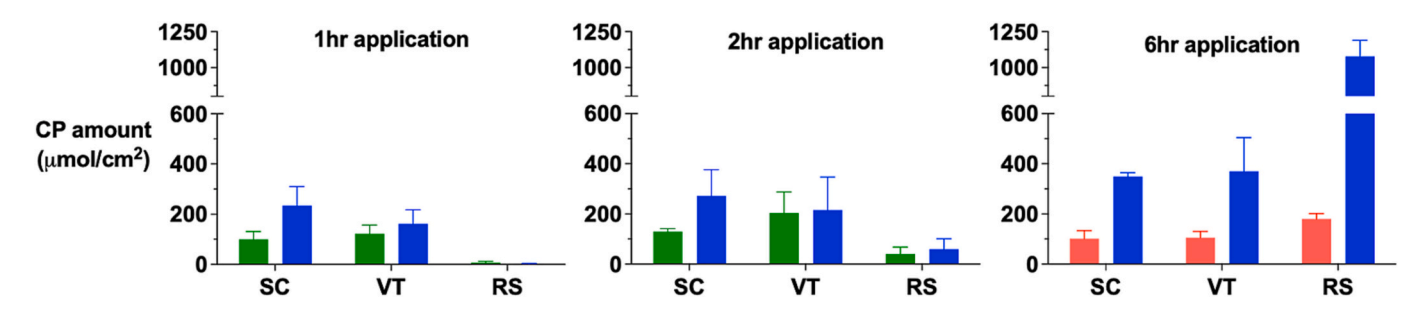


Fig. 10. Disposition of CP in the stratum corneum (SC), viable tissue (VT) and receptor solution (RS) in IVPT experiments post application of three formulations (saturated solutions in 90:10% v/v water:PG (green) and 50:50% v/v water:PG (blue), and 25% saturated solution in 50:50 % v/v water:PG (red)) for 1, 2 or 6 h. Data are the means (\pm SD) of 3 different skin samples from the same pig. (For interpretation of the references to colour in this figure legend, the reader is referred to the web version of this article.)

Table 1 Areas under the normalised CP SRS gray scale profiles as a function of skin depth (AUC_z); calculated from data in Figs. 4 and 7 following application of three water:PG solutions for 1, 2 or 6 h (mean \pm SD of measurements from 6 areas of the same piece of skin).

Experiment		AVIC ()		
CP formulation	Time (h)	AUC _z (μm)		
170 mg/mL in 50:50 v/v water:PG (fully saturated)	1 2 6	$14 \pm 2 \\ 18 \pm 1 \\ 20 \pm 2$		
17 mg/mL in 90:10 v/v water:PG (fully saturated)	1 2	$\begin{array}{c} 7\pm1 \\ 13\pm1 \end{array}$		
42.5 mg/mL in 50:50 v/v water:PG (25% saturated)	6	3 ± 1		

confocal Raman experiments [3] were 2.2 and 2.4. The observation that vehicles with more PG can enhance skin delivery has been attributed to the greater presence of cosolvent delivered into the skin, thereby enabling better solubilisation of the penetrant in the SC [19–21].

When the two 50:50 %v/v water:PG solutions with different degrees of CP saturation after a 6-h application are compared, the AUC_z ratio (fully saturated divided by 25% saturated) was 6.7; that from the confocal Raman study was about 3 [3] – these values bracket and approximate the expected ratio of 4, a reasonable outcome given the relatively limited number of skin samples that have been studied so far: for each formulation and duration, the SRS data comprise 6 measurements from the same skin sample, while the confocal Raman study recorded 6 replicates (1 measurement from 6 different skin samples). This reiterates the point that more replicates, particularly with respect to the SRS measurements being made on multiple skin samples, should reduce both intra-and inter-sample variability.

The SRS results and the previously reported confocal Raman findings may also be compared here to data generated from conventional IVPT experiments, specifically the sum of the amounts recovered in the SC and in the remainder of the skin (referred to as VT in Fig. 10). These

 ν alues, of course, should be correlated in some fashion to the AUC_z results discussed above (however, as the Raman measurements cannot 'report' on the amount of penetrant that has crossed the skin and reached the receptor solution, these quantities were not included in the comparison). The relevant IVPT data are in Table 2.

Once more, it is evident in the IVPT results (and consistent with confocal Raman and SRS results) that the fully saturated CP solution in 50:50 %v/v water:PG delivers more CP into the skin (i.e., SC + VT) than the 90:10, specifically by 1.8-fold and 1.5-fold at 1 and 2 h, respectively. These differences are most important in the SC – in which the corresponding increases are respectively 2.3-fold at 1 h and 2.1-fold at 2 h. The IVPT experiments also captured the SRS (and confocal Raman) differences observed in terms of CP uptake from the fully- and 25%-saturated solutions in 50:50 %v/v water:PG, for which the ratio of [SC + VT] [1] observed was 3.5, in good agreement with the expected value of 4. These comparisons are summarised in Table 3.

As well as permitting a semi-quantitative identification of a chemical's distribution on and within the epidermis/dermis — and insight into the permeation mechanism — SRS imaging can identify specific structural components in different parts of the skin. A representative

Table 2 CP quantities recovered in the stratum corneum (SC) and the remaining skin layers (VT) (and the sums thereof) in a series of IVPT experiments following application of three water: PG solutions for 1, 2 or 6 h (mean \pm SD of 3 skin samples from one pig). The values for SC + VT were first determined for each of the three replicates and the mean \pm SD of these sums were then calculated (it should be noted that the SD of these summed values can be higher or lower when the two measurements are 'pooled' together).

Experiment		CP quantities (µg cm ⁻²)			
CP formulation	Time (h)	SC	VT	SC + VT	
170 mg/mL in 50:50 v/v water:PG (fully saturated)	1	235 ± 75	163 ± 55	398 ± 121	
	2	273 ± 105	216 ± 132	489 ± 182	
	6	350 ± 15	371 ± 135	720 ± 137	
17 mg/mL in 90:10 v/v water:PG (fully saturated)	1	100 ± 31	123 ± 33	224 ± 52	
	2	130 ± 12	205 ± 83	335 ± 82	
42.5 mg/mL in 50:50 v/v water:PG (25% saturated)	6	102 ± 33	106 ± 26	208 ± 23	

Table 3
Ratios of AUC_z from the SRS and confocal Raman experiments compared with the ratios of the quantities recovered in the stratum corneum (SC) alone or combined with the remaining skin layers (VT) in the IVPT experiments following application of three water:PG solutions for 1, 2 or 6 h (SRS: mean of measurements from 6 areas of the same piece of skin; confocal Raman: mean of measurements from 6 different pieces of skin; IVPT: mean of 3 skin samples from one pig).

CP formulations compared		Time (h)		Ratio A/B			
A	В		SRS AUC _z	Confocal AUC _z	IVPT SC+VT	IVPT SC	
170 mg/mL in 50:50 v/v water:PG (saturated)	17 mg/mL in 90:10 v/v water:PG (saturated)	1 2	2.0 1.4	2.2 2.4	1.8 1.5	2.4 2.1	
170 mg/mL in 50:50 v/v water:PG (saturated)	42.5 mg/mL in 50:50 v/v water:PG (25% saturated)	6	6.7	~3	3.5	3.4	

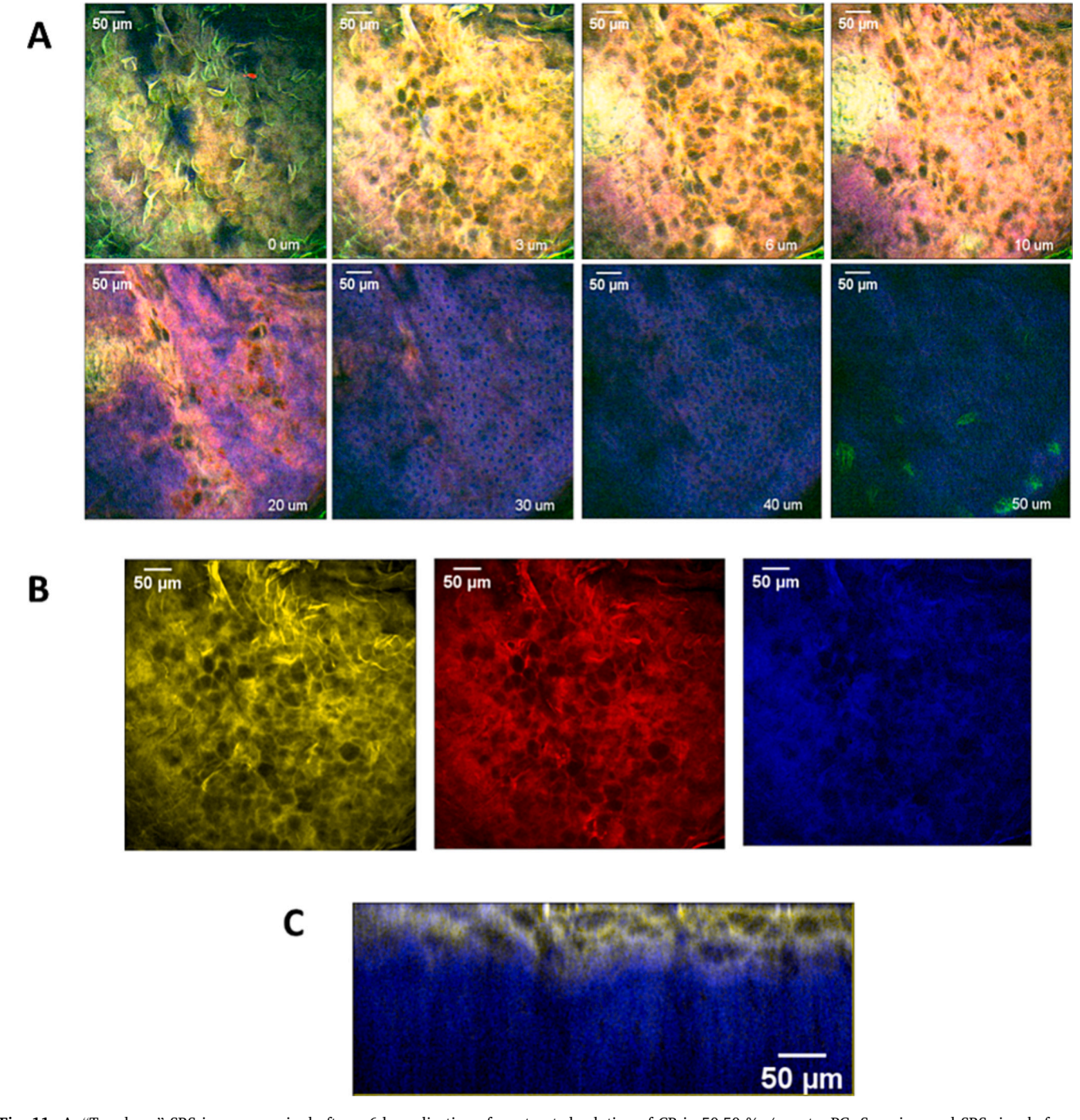


Fig. 11. A. "Top-down" SRS images acquired after a 6-h application of a saturated solution of CP in 50:50 %v/v water:PG. Superimposed SRS signals from CP (yellow), CH₂ (red) and Amide I (blue) are shown as a function of depth into the skin. B. Individual CP, CH₂, and Amide I signals at 3 μ m depth. C. Orthogonal cross-sections - to depths of $\sim 50 \, \mu$ m - of "top-down" SRS images acquired after application of the saturated CP solution for 6 h. Signals from CP (yellow) and Amide I (blue) are shown. All scale bars represent 50 μ m. (For interpretation of the references to colour in this figure legend, the reader is referred to the web version of this article.)

illustration of this capability is provided in the series of SRS images obtained as a function of depth into the skin following application of the 50:50 %v/v water:PG saturated solution of CP for 6 h (Fig. 11 A).

Flattened and elongated corneocytes (10– $40\,\mu m$ in width) are observed in the SC. SRS signals from within these terminally differentiated cells are relatively low as has been reported previously (Osseiran et al., 2018). In contrast, the intercellular lipids (the 'mortar' between the corneocyte 'bricks') are clearly visualised, consistent with the expected partitioning between the lipids and corneocytes based on the octanol-water partition coefficient (\sim 40). This is reflected by the intense orange colouring of the intercellular space generated from the overlap

between the yellow-labelled CP and the red-labelling of the SC lipid domains. Fig. 11B, acquired at a depth of 3 μm into the SC highlights this juxtaposition, and confirms the weak signals originating from within the corneocytes. The larger presence of CP in the intercellular lipids can also be appreciated in the orthogonal cross-sections (Fig. 11C) created by optically slicing through the series of 'top-down' images (exemplified by those in Fig. 11 A). Beyond the SC, Fig. 11 A shows how the size and shape of the keratinocytes evolve within the viable epidermis [9]. The transition from a smaller, spherical appearance at 30–50 μm in depth to the more flattened shape as the SC is approached can be observed.

5. Conclusions

This research has achieved the two major objectives of the project. First, the anticipated advantages of SRS microscopy have been demonstrated: specifically, enabling a finer precision with respect to measurements made within the skin as a function of depth, an ability to image larger areas of skin with different topographies, and in visualizing the relative amounts of a model chemical probe in the lipids and corneocytes. Second, SRS can also detect and distinguish between chemical uptake into the skin from different formulations of the model compound applied for different periods of time, confirming earlier findings from a more conventional confocal Raman spectroscopy technique. In terms of the amount of chemical determined spectroscopically to be within the skin, a good correlation with classic IVPT analysis was also demonstrated. Further work aims to capitalize on the results presented here and to explore the capabilities of SRS to monitor the skin permeation of APIs, applied in approved drug products, and used in the treatment of dermatological diseases.

Supplementary data to this article can be found online at https://doi.org/10.1016/j.jconrel.2024.02.011.

CRediT authorship contribution statement

Panagiota Zarmpi: Writing - review & editing, Writing - original draft, Methodology, Investigation, Data curation, Conceptualization. Dimitrios Tsikritsis: Writing - review & editing, Writing - original draft, Visualization, Methodology, Investigation, Conceptualization. Jean-Luc Vorng: Writing - review & editing, Visualization, Methodology, Investigation. Natalie A. Belsey: Writing - review & editing, Writing - original draft, Visualization, Supervision, Methodology, Investigation, Funding acquisition, Conceptualization. Annette L. Bunge: Writing - review & editing, Writing - original draft, Validation, Supervision, Methodology, Investigation, Funding acquisition, Conceptualization. Timothy J. Woodman: Writing - review & editing, Writing - original draft, Methodology, Investigation. M. Begoña Delgado-Charro: Writing - review & editing, Writing - original draft, Validation, Supervision, Methodology, Investigation, Funding acquisition, Conceptualization. Richard H. Guy: Writing - review & editing, Writing original draft, Visualization, Validation, Supervision, Project administration, Methodology, Investigation, **Funding** acquisition, Conceptualization.

Declaration of competing interest

None.

Data availability

Data will be made available on request.

Acknowledgements

This project is supported by the Food and Drug Administration (FDA) of the U.S. Department of Health and Human Services (HHS) as part of a financial assistance award (1-U01-FD 006533) totalling \$1.25 M with 100% funded by FDA]/HHS. The contents are those of the author(s) and do not necessarily represent the official views of, nor an endorsement, by FDA/HHS, or the U.S. Government. Valuable insight from and stimulating discussions with Drs. Priyanka Ghosh, Sam Raney and Markham Luke from the FDA's Office of Generic Drugs, and from Professor Jane White at the University of Bath, are gratefully acknowledged. NAB thanks the Community for Analytical Measurement Science for a 2020 CAMS Fellowship Award funded by the Analytical Chemistry Trust

Fund.

References

- [1] A. Feizpour, T. Marstrand, L. Bastholm, S. Eirefelt, C.L. Evans, Label-free quantification of pharmacokinetics in skin with stimulated Raman scattering microscopy and deep learning, J. Invest. Dermatol. 141 (2021) 395–403, https:// doi.org/10.1016/j.jid.2020.06.027.
- [2] M.A. Maciel Tabosa, P. Vitry, P. Zarmpi, A.L. Bunge, N.A. Belsey, D. Tsikritsis, T. J. Woodman, K.A.J. White, M.B. Delgado-Charro, R.H. Guy, Quantification of chemical uptake into the skin by vibrational spectroscopies and stratum Corneum sampling, Mol. Pharm. 20 (2023) 2527–2535, https://doi.org/10.1021/acs.molpharmaceut 2c01109
- [3] P. Zarmpi, M.A.M. Tabosa, P. Vitry, A.L. Bunge, N.A. Belsey, D. Tsikritsis, T. J. Woodman, M.B. Delgado-Charro, R.H. Guy, Confocal Raman spectroscopic characterization of Dermatopharmacokinetics ex vivo, Mol. Pharm. 20 (2023) 5910–5920, https://doi.org/10.1021/acs.molpharmaceut.3c00755.
- [4] FDA, FY 2022 GDUFA Science And Research Report. https://www.fda.gov/media/164843/download, 2022 (accessed 28 October 2023).
- [5] D. Tsikritsis, E.J. Legge, N.A. Belsey, Practical considerations for quantitative and reproducible measurements with stimulated Raman scattering microscopy, Analyst 147 (2022) 4642–4656, https://doi.org/10.1039/D2AN00817C.
- [6] N.A. Belsey, N.L. Garrett, L.R. Contreras-Rojas, A.J. Pickup-Gerlaugh, G.J. Price, J. Moger, R.H. Guy, Evaluation of drug delivery to intact and Porated skin by coherent Raman scattering and fluorescence microscopies, J. Control. Release 174 (2014) 37–42. https://doi.org/10.1016/j.iconrel.2013.11.002.
- [7] B.G. Saar, L.R. Contreras-Rojas, X.S. Xie, R.H. Guy, Imaging drug delivery to skin with stimulated Raman scattering microscopy, Mol. Pharm. 8 (2011) 969–975, https://doi.org/10.1021/mp.200122w.
- [8] W.S. Chiu, N.A. Belsey, N.L. Garrett, J. Moger, M.B. Delgado-Charro, R.H. Guy, Molecular diffusion in the human nail measured by stimulated Raman scattering microscopy, Proc. Natl. Acad. Sci. USA 112 (2015) 7725–7730, https://doi.org/ 10.1073/pnas.1503791112.
- [9] M. Egawa, S. Iwanaga, J. Hosoi, M. Goto, H. Yamanishi, M. Miyai, C. Katagiri, K. Tokunaga, T. Asai, Y. Ozeki, Label-free stimulated Raman scattering microscopy visualizes changes in intracellular morphology during human epidermal keratinocyte differentiation, Sci. Rep. 9 (2019) 12601, https://doi.org/10.1038/ s41598.019.49035.x
- [10] S. Osseiran, J.D. Cruz, S. Jeong, H. Wang, C. Fthenakis, C.L. Evans, Characterizing stratum corneum structure, barrier function, and chemical content of human skin with coherent Raman scattering imaging, Biomed. Opt. Express 9 (2018) 6425–6443, https://doi.org/10.1364/BOE.9.006425.
- [11] A. Goel, D. Tsikritsis, N.A. Belsey, R. Pendlington, S. Glavin, T. Chen, Measurement of chemical penetration in skin using stimulated Raman scattering microscopy and multivariate curve resolution - alternating least squares, Spectrochim. Acta A Mol. Biomol. Spectrosc. 296 (2023) 122639, https://doi.org/10.1016/j. saa.2023.122639
- [12] C.A. Schneider, W.S. Rasband, K.W. Eliceiri, NIH image to ImageJ: 25 years of image analysis, Nat. Methods 9 (2012) 671–675, https://doi.org/10.1038/ nmeth.2089.
- [13] A. Pappas, S. Johnsen, J.C. Liu, M. Eisinger, Sebum analysis of individuals with and without acne, Dermatoendocrinol. 1 (2009) 157–161, https://doi.org/10.4161/ derm. 1.3.8473
- [14] X. Chen, O. Nadiarynkh, S. Plotnikov, P.J. Campagnola, Second harmonic generation microscopy for quantitative analysis of collagen fibrillar structure, Nat. Protoc. 7 (2012) 654–669, https://doi.org/10.1038/nprot.2012.009.
- [15] P.-C. Wu, T.-Y. Hsieh, Z.-U. Tsai, T.-M. Liu, In vivo quantification of the structural changes of collagens in a melanoma microenvironment with second and third harmonic generation microscopy, Sci. Rep. 5 (2015) 8879, https://doi.org/ 10.1038/srep08879.
- [16] F. Pirot, Y.N. Kalia, A.L. Stinchcomb, G. Keating, A. Bunge, R.H. Guy, Characterization of the permeability barrier of human skin *in vivo*, Proc. Natl. Acad. Sci. USA 94 (1997) 1562–1567, https://doi.org/10.1073/pnas.94.4.1562.
- [17] B. Sarri, X. Chen, R. Canonge, S. Grégoire, F. Formanek, J.-B. Galey, A. Potter, T. Bornschlögl, H. Rigneault, In vivo quantitative molecular absorption of glycerol in human skin using coherent anti-stokes Raman scattering (CARS) and two-photon auto-fluorescence, J. Control. Release 308 (2019) 190–196, https://doi.org/ 10.1016/j.jconrel.2019.07.018.
- [18] S. Mitragotri, Modeling skin permeability to hydrophilic and hydrophobic solutes based on four permeation pathways, J. Control. Release 86 (2003) 69–92, https://doi.org/10.1016/s0168-3659(02)00321-8.
- [19] S. Nicoli, A.L. Bunge, M.B. Delgado-Charro, R.H. Guy, Dermatopharmacokinetics: factors influencing drug clearance from the stratum Corneum, Pharm. Res. 26 (2009) 865–871, https://doi.org/10.1007/s11095-008-9785-y.
- [20] C. Herkenne, A. Naik, Y.N. Kalia, J. Hadgraft, R.H. Guy, Effect of propylene glycol on ibuprofen absorption into human skin in vivo, J. Pharm. Sci. 97 (2008) 185–197, https://doi.org/10.1002/jps.20829.
- [21] R.H. Guy, A.F. Davis, Topical drug delivery, in: C.E.M. Griffiths, J. Barker, T. O. Bleiker, W. Hussain, R.C. Simpson (Eds.), Rook's Textbook of Dermatology, John Wiley & Sons, Ltd, Chichester, U.K., 2024.